Electromagnectic Scattering from Ocean Surface

Phuc Tran
Code 4T4400D
Research Department
Naval Air Warfare Center Weapons Division

Abstract

We describe our efforts in the last few years to develop electromagnetic scattering code using the computers at the DoD High Performance Computing Modernization Project sites. In particular, a FFT-MOMI technique for the scattering of EM waves from a perfectly conducting surface will be discussed.

Introduction

Ship self-defense is a major area of concern for the Navy since an expensive asset (a ship) can be destroyed by an inexpensive (relative to the cost of the ship) sea-skimming missile. Therefore, the ability to detect incoming sea-skimming cruise missile is critical. However, detection is very difficult because of multi-path effects from the sea surface. That is the radar return from the missile contains the radiation that not only scattered off the missile directly back to the receiver but also scattered off the missile then off the sea surface before reaching the receiver. The interplay amongst these scattering mechanisms makes it very difficult to know if there is a target out there. A secondary problem that is also of interest is the reverse problem, i.e. how does a sea-skimming cruise missile find its target. The missile in essence has the same problem as the ship. Therefore, in the end game, the missile must execute a pop-up maneuver to find its target. This exposes the missile to ship self-defense system, which is undesirable. An understanding of the sea surface scattering problem therefore will aid in the design of detection system for both ship and missile.

The scattering of electromagnetic radiation from the sea surface is a computationally demanding problem because it is an unbounded problem. Particularly, in the grazing geometry that one encounters in the sea-skimming scenario, the footprint or illuminated area approaches infinity. In practice, one confines the calculation domain to a finite surface; however, the surface must be big enough to retain the essential features of the problem, e.g. shadowing effects. Even then the size of the surface still poses computationally challenging problems. In this paper, we describe some of our efforts in the last few years to develop an efficient electromagnetic waves surface scattering code. The calculations were done using computer resources from the High Performance Computing Modernization Program centers (ASECC at NUWC, ERDC, and NAVO).

EM Scattering and Integral Equation

An integral formulation is often employed in the solution of the electromagnetic scattering from a surface. Generally this means that the current on the surface is expressed in terms of an integral equation from which it is to be determined, i.e.

$$\mathbf{J} = \mathbf{J}_0(\mathbf{R}) + \int \mathbf{K}(\mathbf{r},\mathbf{r}')\mathbf{J}(\mathbf{R}')d\mathbf{S}' , \qquad (1)$$

where **J** is the unknown surface current, $\mathbf{J}_0$ is the current generated by the incident field, **K** is the kernel, and the integral is over the surface. We have used the notation **r** = (**R**,z) with **R** = (x,y). The surface to be assumed to be describable by a function $z = V(x,y) = V(\mathbf{R})$. Once the surface current is determined, the scattered field can be calculated from it. Solving Eq. (1) is the most demanding part of the scattering problem. Equation (1) is converted to a matrix equation $\mathbf{J} = \mathbf{J}_0 + \mathbf{K}\mathbf{J}$, and usually some form of conjugate gradient technique is employed to get the solution. Essentially, an initial guess to the solution is used to start the conjugate gradient process. This guess is inserted into the right hand side of the matrix equation to calculate the left hand side. There will be error, and a correction to the initial guess will be calculated. Then the process repeats itself until the error reaches a tolerance limit.

The most time consuming step in the above procedure is the matrix-vector multiplication. Since **K** is a square matrix with *NxN* elements and **J** is a vector with *N* elements where *N* is the number of unknowns, this step requires N^2 operations in general. Consider a surface of the size 100λx100λ where λ is the radiation wavelength. This surface will have at least $N = 10^6$ unknown (this is based upon a conservative discretization of the surface into 0.1λx0.1λ patches). One can see that this can be very time consuming. A second aspect of the conjugate gradient method that is undesirable is the slow convergence, i.e. it can take hundreds of iteration for the solution to converge. In this paper, we describe a combination of two techniques to address the above two issues. The first is a FFT technique to perform the matrix-vector product that scales as *NlnN*. This technique was developed by Tsang *et al.* [1]. The second is a fast convergent iterative method called the Method of Ordered Multiple Interactions (MOMI) developed by Kapp and Brown [2]. Also, we discuss how parallel implementation can be done.

FFT Matrix-Vector Multiplication

To illustrate the technique of FFT matrix-vector multiplication [1], we need a concrete example, so we use here the problem of electromagnetic scattering from a perfectly conducting surface. Although this is for illustrative purposes, this model can be useful for radar scattering from ocean surface since it is a good first approximation (radar does not penetrate very well into the ocean). The surface current, $\mathbf{j} = \mathbf{n} \times \mathbf{H}$, is given by the integral equation

$$\mathbf{j}(\mathbf{R}) = 2\mathbf{j}^{inc}(\mathbf{R}) + \frac{1}{2p}\mathbf{n}(\mathbf{R}) \times \wp \int \left[\nabla G_o(\mathbf{R},\mathbf{R}') \times \mathbf{j}(\mathbf{R}')\right] d^2R' \qquad (2)$$

where

$\mathbf{n} = [\hat{z} - \nabla V(\mathbf{R})]$ is the surface normal and $G_o(\mathbf{r},\mathbf{r}') = \exp[i(w/c)|\mathbf{r}-\mathbf{r}'|]/|\mathbf{r}-\mathbf{r}'|$ is the free space Green's function. The idea of FFT matrix-vector multiplication is to express the integral in Eq. (2) in convolution form for which the product can be done in Fourier space. For this purpose, the integral is broken into two regions, a near and far region as defined by a cutoff distance

$$\int [\nabla G_o(\mathbf{R},\mathbf{R}') \times \mathbf{j}(\mathbf{R}')] d^2R' = \int_{|\mathbf{R}-\mathbf{R}'|<cutoff} [\nabla G_o(\mathbf{R},\mathbf{R}') \times \mathbf{j}(\mathbf{R}')] d^2R' + \int_{|\mathbf{R}-\mathbf{R}'|\geq cutoff} [\nabla G_o(\mathbf{R},\mathbf{R}') \times \mathbf{j}(\mathbf{R}')] d^2R' . \quad (3)$$

The second integral on the right hand side of Eq. (3) is called the far region, and it will be rewritten in convolution form by expanding the kernel in a Taylor series around the point $a \equiv [V(\mathbf{R}) - V(\mathbf{R}')]^2 = 0$. Using the definition for the Green's function G_0 and $|\mathbf{r}-\mathbf{r}'| = \sqrt{(\mathbf{R}-\mathbf{R}')^2 + [V(\mathbf{R}) - V(\mathbf{R}')]^2}$ we get

$$\nabla G_0(\mathbf{r},\mathbf{r}') = \sum_{n=0}^{\infty} \frac{1}{n!} \frac{d^n[\nabla G_0(\mathbf{r},\mathbf{r}')]}{da^n}\bigg|_{a=0} a^n . \quad (4)$$

The Taylor series is truncated at some n. Expanding the term a^n we get terms of the form $V(\mathbf{R})^j V(\mathbf{R}')^k$, while the derivative term has only the dependence $|\mathbf{R}-\mathbf{R}'|$ (since it is evaluated at $a = 0$). Substituting Eq. (4) into the second term on the right hand side of Eq. (3), we get various terms of the convolution form

$$\int f(\mathbf{R}) g(\mathbf{R}-\mathbf{R}') h(\mathbf{R}') dR' . \quad (5)$$

Integral of the convolution form can be done by FFT to Fourier space where the convolution is just a product that can be done in N operation. The $NlnN$ scaling comes from the FFT itself.

The first integral in the right hand side of Eq. (3), corresponding to the near region, is calculated the standard way, i.e. no convolution. Therefore, to minimize the near region calculation, the cutoff distance is chosen so that this region is small compared to the far region. The choice of the cutoff distance will of course effect the Taylor expansion. It determines how many terms to keep in the Taylor series expansion to achieve a specific error tolerance.

Method of Ordered Multiple Interaction (MOMI)

In this section we describe the Method of Ordered Multiple Interactions (MOMI) [2], how it can be parallelized, and how the FFT matrix-vector approach can be

incorporated. Unlike the conjugate gradient approach, the MOMI utilizes a Neumann iteration technique. In this approach, the incident current is taken as the initial guess. The unknown surface current is then calculated. This current is then used as the next guess, i.e. $\mathbf{J}_n = \mathbf{J}^{inc} + \mathbf{K}\mathbf{J}_{n-1}$. The solution obtained this way can be written as a series,

$$\mathbf{J} = \mathbf{J}^{inc} + \mathbf{K}\mathbf{J}^{inc} + \mathbf{K}^2\mathbf{J}^{inc} + \mathbf{K}^3\mathbf{J}^{inc} + \ldots \tag{6}$$

The MOMI uses the Neumann iteration on a modified form of the matrix equation. First, the kernel **K** is broken into a lower and upper matrix **K** = **L** + **U**. Note that we assume there is no diagonal part **D** because this can always be separated, bought over to the left hand side, and renormalize everything by (**I**-**D**). The matrix equation can now be written in terms of the **L** and **U** matrices as follows

$$\mathbf{J} = (\mathbf{I} - \mathbf{U})^{-1}(\mathbf{I} - \mathbf{L})^{-1}\mathbf{J}^{inc} + (\mathbf{I} - \mathbf{U})^{-1}(\mathbf{I} - \mathbf{L})^{-1}\mathbf{L}\mathbf{U}\mathbf{J}. \tag{7}$$

Applying the Neumann iteration to Eq. (7) we get the series solution

$$\mathbf{J} = (\mathbf{I} - \mathbf{U})^{-1}\left[\mathbf{I} + \sum_{n=1}^{\infty}\left\{(\mathbf{I} - \mathbf{L})^{-1}\mathbf{L}\mathbf{U}(\mathbf{I} - \mathbf{U})^{-1}\right\}^n\right](\mathbf{I} - \mathbf{L})^{-1}\mathbf{J}^{inc}. \tag{8}$$

Coupled with the identities $(\mathbf{I} - \mathbf{L})^{-1}\mathbf{L} = (\mathbf{I} - \mathbf{L})^{-1} - \mathbf{I}$ and $\mathbf{U}(\mathbf{I} - \mathbf{U})^{-1} = (\mathbf{I} - \mathbf{U})^{-1} - \mathbf{I}$, the solution for the surface current is given now in terms of two matrices $(\mathbf{I} - \mathbf{L})^{-1}$ and $(\mathbf{I} - \mathbf{U})^{-1}$ only. Although these two matrices require an inversion, there is no need for explicitly calculating them because they are always multiplied with a vector, which can be done using forward and backward substitution. To illustrate this point, let us look at how to evaluate $\mathbf{X} = (\mathbf{I} - \mathbf{L})^{-1}\mathbf{A}$ where **A** is a known vector. This equation is equivalent to $(\mathbf{I} - \mathbf{L})\mathbf{X} = \mathbf{A}$. Because of the nature of the matrix **L** (a lower triangular matrix), we get the following set of equations

$$\begin{aligned}
X_1 &= A_1 \\
X_2 &= A_2 + L_{21}X_1 \\
X_3 &= A_3 + L_{32}X_2 + L_{31}X_1 \\
&\vdots \\
X_n &= A_n + \sum_{m<n} L_{nm}X_m
\end{aligned} \tag{9}$$

From Eq. (9) we see that we can calculate the *m*th element if we know all the element preceeding it. Starting from the first element, whose solution is trivial, we can sequentially determine the rest (hence the name forward substitution). For the other matrix $(\mathbf{I} - \mathbf{U})^{-1}$, the same is true except the order is reversed, i.e. we start from the last element and work backward (backward substitution).

The operation count of Eq. (9) is of order N^2. However, most of these can be performed in parallel. To see this, note that once X_1 is known the product $L_{m1}X_1$ for all m can be calculated in parallel. This is how we implement the MOMI solution to take advantage of the parallel computer. The reason we use the solution given by Eq. (8) instead of that of Eq. (6) is that the former converges faster for the same amount of computational efforts. To understand the origin for this, let us look at the physical interpretation of the terms in both equations.

The successive term on the right hand side of Eq. (6) describes a unique scattering process on the surface. The first term is just the current due to the incident wave. The second term corresponds to current due to the singly scattered waves from another point on the surface. The term $\mathbf{K}^n\mathbf{J}^{inc}$ describes the current due to n-scattered waves. Now let us look at Eq. (8). As stated before, this series solution is expressible in terms of only two matrices, $(\mathbf{I}-\mathbf{L})^{-1} \equiv \mathbf{I}+\underline{\mathbf{L}}$ and $(\mathbf{I}-\mathbf{U})^{-1} \equiv \mathbf{I}+\underline{\mathbf{U}}$. For interpretational purposes, we have defined two new matrices $\underline{\mathbf{L}}$ and $\underline{\mathbf{U}}$. What is the physical meaning of these two new matrices? From their definition, we can solve for them in terms of $\mathbf{L}$ and $\mathbf{U}$, but their meaning can be understood most easily from the diagrams in Fig. (1). Unlike the matrix $\mathbf{L}$ or $\mathbf{U}$, where each instance of occurrence of either one corresponds to an additional scattering between two points on the surface, each occurrence of $\underline{\mathbf{L}}$ or $\underline{\mathbf{U}}$ corresponds to a set of scattering processes. Between two points, the $\underline{\mathbf{L}}$ ($\underline{\mathbf{U}}$) matrix represents all possible scattering processes going forward (backward). The only restriction is that in either case, reversal of direction is not allowed. This restriction is why the method is known as the Method of Ordered Multiple Interactions (MOMI). The top diagram in Fig. (1) shows the matrix element (blue line) corresponding to $\underline{\mathbf{L}}$ (left diagram) and $\underline{\mathbf{U}}$ (right diagram) connecting two elements of a vector $\mathbf{J}$. Below these diagrams are the equivalent description in terms of the $\mathbf{L}$ and $\mathbf{U}$ matrices (red lines). Note that we have shown only two possible processes to illustrate our point. To get the true equivalent, we must include all possible ways to go between the two points without reversing the arrow direction. This explains why the MOMI solution is more robust than that of Eq. (6). The first term in Eq. (8), which is called the Born term, can be written in terms of the $\underline{\mathbf{L}}$ and $\underline{\mathbf{U}}$ matrices as

$$\mathbf{J}_{born} = (\mathbf{I}+\underline{\mathbf{U}})(\mathbf{I}+\underline{\mathbf{L}})\mathbf{J}^{inc}. \qquad (10)$$

With the interpretation of the two matrices described in Fig. (1), we see that even this term already includes many more scattering processes; some of these are included only after many iterations of Eq. (6).

FFT-MOMI

In this section, we describe how the FFT matrix-vector multiplication can be combined with the MOMI. To see how this can be accomplished, let us look at how to calculate $\mathbf{X} = (\mathbf{I}-\mathbf{L})^{-1}\mathbf{A}$ again, but this time we re-express it in terms of sub-vectors, i.e. $\mathbf{X} = \sum_m \mathbf{x}_m$. In terms of these sub-vectors, we get an equation analogous to Eq. (9)

$$\mathbf{x}_n = \left(\mathbf{I} - \mathbf{L}_{nn}\right)^{-1}\left[\mathbf{a}_n + \sum_{m<n}\mathbf{L}_{nm}\mathbf{x}_m\right]. \qquad (11)$$

The second term in the square bracket of Eq. (10) is now a matrix-vector product which the FFT technique can be applied. The next question we need to address is how to define the sub-vectors so that the FFT technique can be applied. Since the convolution integral in the FFT technique requires a well-defined distance vector (**R**-**R**'), a natural sub-vector is a subsection of the surface. A simple scheme then is to divide the surface into square sections and to assign each section to a sub-vector. The remaining question is how to number these regions. We found the following numbering scheme (as shown in Fig. (2)) the most economical in terms of keeping the number and size of the FFT to a minimal. As shown in Fig. (2), the surface is divided into 4 sections. Each section is then divided into 4 again. This is repeated until a desired size is reached. The numbering starts with the smallest unit. They are numbered consecutively until one reaches a larger region. This region is now one fourth of a larger region. The numbering continues on the other 3/4 of this larger region as shown in Fig. (2). This process is continued to larger level. Equation (11) would be calculated as follows. The first region $\mathbf{x}_1$ is calculated by forward substitution. Then the product $\mathbf{L}_{21}\mathbf{x}_1$, $\mathbf{L}_{31}\mathbf{x}_1$, and $\mathbf{L}_{41}\mathbf{x}_1$ are calculated using FFT. The rest of the procedure is the same keeping in mind that at any step the FFT size should be minimized.

Sample Calculation and Discussion

In this section we give some results using the above method to calculate the scattering of electromagnetic waves from a randomly rough perfectly conducting surface. The random surface is generated using the algorithm in ref. [3]. The root mean square height of the surface is $\sigma = 0.75\lambda$, and the lateral correlation length is $a = 2.0\lambda$ where λ is the radiation wavelength. The surface is of the size $25.6\lambda \times 25.6\lambda$. The surface is discretized into $0.1\lambda \times 0.1\lambda$ patches. The incident field is a sum of plane waves [4] with a nominal incident angle of 45^o. The incident field is p-polarized. The differential reflection coefficient (DRC) or the scattered power per solid angle $dP(J,f)/d\Omega$ normalized to the incident power is calculated and shown in Fig. (3). In Fig. (3a), we show the in-plane ($\phi = 0^o$) co-polarized DRC calculated from the Born term, i.e. Eq. (10). Two different calculations are shown. The black curve corresponds to the case where the surface is not divided into sub sections and no FFT matrix-vector calculation was used. The red curve corresponds to the case where the surface is divided into 64 sub regions as shown in Fig. (2). In Fig. (3b), we shown the DRC calculated from 3 iterations of Eq. (8). There are several points to note. Even though the DRC shows some discrepancies, when comparing both cases, with only the Born term, they both converge to the same DRC after 3 iterations. The convergence rate of 3 iterations with 3 digit accuracy is very fast (illustrating the advantage of the MOMI). Comparison of Figs. (3a) and (3b) shows that the DRC based upon Born term is quite good.

For the above calculations, the FFT-MOMI required longer CPU time compare to the MOMI because there is FFT overhead that must be overcomed. We have looked at

the scaling of the FFT-MOMI as a function of N, and it is slightly larger than the $NlnN$. We were able to exploit the inherent parallel nature of the forward and backward substitution and take advantage of parallel computers. Unfortunately, we have not employed a parallel FFT routine. Having a parallel FFT routine would significantly enhance the FFT-MOMI as FFT is the dominant time consuming steps in the process.

In conclusion, we have described a problem of interest to the Navy, the detection of sea-skimming cruise missile, that stands to benefit from the computers being made available through High Performance Computing Modernization Program. This problem requires an understanding of the scattering of electromagnetic radiation from sea surface, and the computers from the HPCMP provide a tool for the modeling of this problem.

Acknowledgement

We thank the HPCMP, in particular ASECC at NUWC, ERDC, and NAVO, for computer times.

References

[1] L. Tsang, C. H. Chan, and K. Pak, "Monte Carlo simulation of a two-dimensional random rough surface using the sparse-matrix flat-surface iterative approach," Electron. Lett. vol. 29, pp. 1153-1154 (1993); L. Tsang, C. H. Chan, and K. Pak, "Backscattering enhancement of a two-dimensional, random rough surface (three-dimensional scattering) based on Monte Carlo simulations," J. Opt. Soc. Am. A vol. 11, pp. 711-715 (1994).
[2] D. A. Kapp and G. S. Brown, "A New numerical method for rough surface scattering calculations," IEEE Trans. Antennas Propagat. vol. 44, pp. 711-721 (1996).
[3] N. Garcia and E. Stoll, "Monte Carlo calculation for electromagnetic wave scattering from random rough surface," Phys. Rev. Lett. vol. 52, pp. 1798-1801 (1984).
[4] P. Tran and A. A. Maradudin, "The scattering of electromagnetic waves from a randomly rough 2-D metallic surface," Opt. Comm. vol. 110, pp. 269-273 (1994).

Figure Captions

Figure 1: Diagrammatic description of the matrix **L** (top left diagram) and **U** (top right diagram). The dot represents the elements of the vector **J**. The blue line with arrow represents the matrix element **L** and **U**. The lower diagrams show the equivalent (red lines) in terms of the matrix **L** (left diagram) and **U** (right diagram). Note that only two possible processes are shown in the lower diagrams. The true equivalent would be all possible paths connecting two points with the restriction that all arrows must point the same direction.

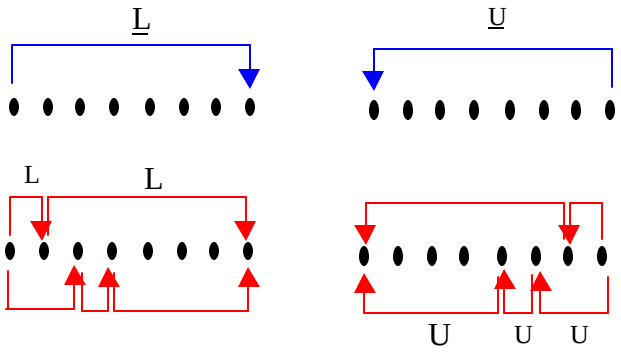

Figure 2: Diagram of how the surface is divided into sub regions and numbered for the FFT-MOMI algorithm.

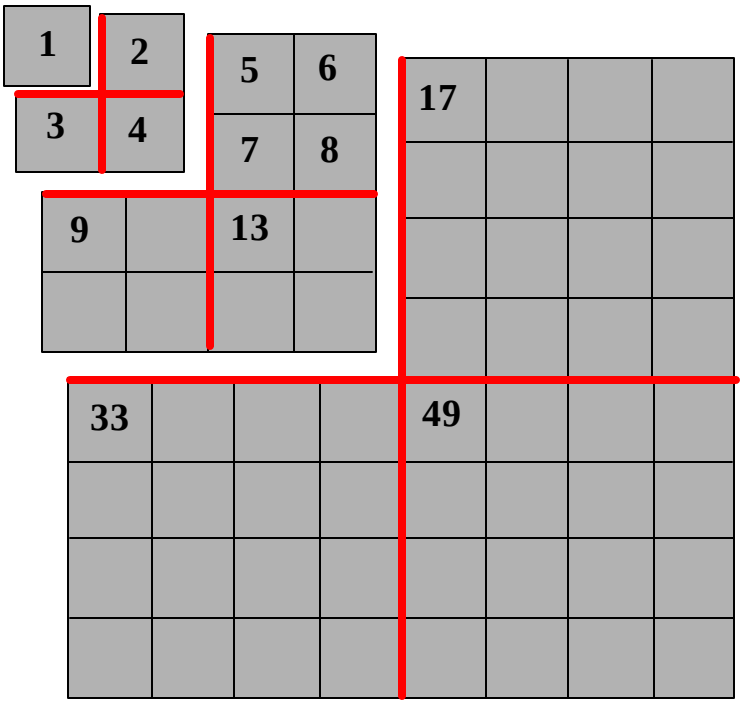

Figure 3: Plot of the Differential Reflection Coefficient (DRC) (a) from the Born term only and (b) from 3 iterations of Eq. (8). The red curve corresponds to the FFT-MOMI with the surface divided into 64 sub regions, and the black curve corresponds to the MOMI (no subdivision of the surface). The two curves are indistinguishable in (b).